Report

Current Biology

Avian neurons consume three times less glucose than mammalian neurons

Highlights

- Brain tissue of awake pigeons consumes 27.29 ± 1.57 μmol glucose per 100 g per min
- This is equal to $1.86 \times 10^{-9} \pm 0.2 \times 10^{-9}$ μmol glucose per neuron per minute
- The neuronal energy budget of pigeons is thus about 3× lower compared to mammals
- This possibly indicates more efficient neuronal processing in the avian clade

Authors

Kaya von Eugen, Heike Endepols, Alexander Drzezga, Bernd Neumaier, Onur Güntürkün, Heiko Backes, Felix Ströckens

Correspondence

felix.stroeckens@hhu.de

In brief

In comparison to mammals, neuron densities in the avian brain are high, opening up the question of how birds can metabolically support their large neuron numbers. Von Eugen et al. show here that the neuronal energy budget of pigeons is about 3 times lower compared to mammals, possibly indicating a more efficient neuronal processing in the avian clade.

von Eugen et al., 2022, Current Biology *32*, 1–8
October 10, 2022
https://doi.org/10.1016/j.cub.2022.07.070

CellPress

Please cite this article in press as: von Eugen et al., Avian neurons consume three times less glucose than mammalian neurons, Current Biology (2022), https://doi.org/10.1016/j.cub.2022.07.070

Current Biology

CellPress

Report

Avian neurons consume three times less glucose than mammalian neurons

Kaya von Eugen,[1] Heike Endepols,[2,3,4] Alexander Drzezga,[2,5,6] Bernd Neumaier,[3,4] Onur Güntürkün,[1] Heiko Backes,[7] and Felix Ströckens[1,8,9,*]

[1]Department of Biopsychology, Institute of Cognitive Neuroscience, Ruhr University Bochum, Bochum, Germany
[2]Department of Nuclear Medicine, Faculty of Medicine and University Hospital of Cologne, Cologne, Germany
[3]Institute of Radiochemistry and Experimental Molecular Imaging, Faculty of Medicine and University Hospital of Cologne, Cologne, Germany
[4]Institute of Neuroscience and Medicine, INM-5: Nuclear Chemistry, Forschungszentrum Jülich GmbH, Jülich, Germany
[5]Institute of Neuroscience and Medicine, INM-2: Molecular Organization of the Brain, Forschungszentrum Jülich GmbH, Jülich, Germany
[6]German Center for Neurodegenerative Diseases (DZNE), Bonn-Cologne, Germany
[7]Max Planck Institute for Metabolism Research, Multimodal Imaging Group, Cologne, Germany
[8]Cécile and Oskar Vogt Institute of Brain Research, University Hospital Düsseldorf, Heinrich-Heine University, Düsseldorf, Germany
[9]Lead contact
*Correspondence: felix.stroeckens@hhu.de
https://doi.org/10.1016/j.cub.2022.07.070

SUMMARY

Brains are among the most energetically costly tissues in the mammalian body.[1] This is predominantly caused by expensive neurons with high glucose demands.[2] Across mammals, the neuronal energy budget appears to be fixed, possibly posing an evolutionary constraint on brain growth.[3–6] Compared to similarly sized mammals, birds have higher numbers of neurons, and this advantage conceivably contributes to their cognitive prowess.[7] We set out to determine the neuronal energy budget of birds to elucidate how they can metabolically support such high numbers of neurons. We estimated glucose metabolism using positron emission tomography (PET) and 2-[^{18}F]fluoro-2-deoxyglucose ([^{18}F]FDG) as the radiotracer in awake and anesthetized pigeons. Combined with kinetic modeling, this is the gold standard to quantify cerebral metabolic rate of glucose consumption (CMR_{glc}).[8] We found that neural tissue in the pigeon consumes 27.29 ± 1.57 μmol glucose per 100 g per min in an awake state, which translates into a surprisingly low neuronal energy budget of $1.86 \times 10^{-9} \pm 0.2 \times 10^{-9}$ μmol glucose per neuron per minute. This is approximately 3 times lower than the rate in the average mammalian neuron.[3] The remarkably low neuronal energy budget explains how pigeons, and possibly other avian species, can support such high numbers of neurons without associated metabolic costs or compromising neuronal signaling. The advantage in neuronal processing of information at a higher efficiency possibly emerged during the distinct evolution of the avian brain.

RESULTS AND DISCUSSION

It has so far not been possible to determine the exact neuronal energy budget *in vivo*. However, decades of work on estimating the cerebral metabolic rate of glucose (CMR_{glc}) have been combined with more recent estimates of neuron numbers to elucidate whether and how the neuronal energy budget varies between species.[3,9] Across mammals, the high costs of neurons have been shown to be relatively invariant, suggesting that there is a fixed budget across species.[3,4] It is thought that this costly budget posed an evolutionary constraint on brain growth, where an increase in numbers of neurons is a trade-off between the metabolic costs incurred and the benefits obtained from higher information processing capacities.[5,6] Recently, it was found that bird brains contain higher numbers of neurons compared to similarly sized mammalian brains. For some species, these numbers even surpass primates: within a similar volume, the brains of members of the corvids and parrots contain more than twice the number of neurons.[7] Possibly, this enables these small-brained clades to be cognitively on a par with mammals and in some cases, even primates.[10] But how are birds able to sustain such high numbers of neurons?

To address this question, our study set out to establish the glucose needs of brain tissue in pigeons (*Columba livia*), a common model organism in cognitive neuroscience. Since anesthesia is known to have a strong inhibiting effect on cerebral glucose metabolism,[8] we established a method to estimate CMR_{glc} in both anesthetized and awake subjects. Glucose metabolism was assessed using positron emission tomography (PET) and an intravenous (i.v.) injection of the radioactively labeled glucose analog 2-[^{18}F]fluoro-2-deoxyglucose ([^{18}F]FDG) (Figure 1A). Next, the single kinetic rate constants of cerebral [^{18}F]FDG metabolism were determined with a two-tissue compartment model[11] (Figure 1B). The input parameters for the model were the time-activity curve (TAC) in brain tissue and [^{18}F]FDG values in arterial plasma over time, known as the arterial input function (AIF). The final local CMR_{glc} was calculated from the local kinetic rate constants of [^{18}F]FDG taking into account differences in transport and phosphorylation of glucose and [^{18}F]FDG,[12–14] multiplied by

Please cite this article in press as: von Eugen et al., Avian neurons consume three times less glucose than mammalian neurons, Current Biology (2022), https://doi.org/10.1016/j.cub.2022.07.070

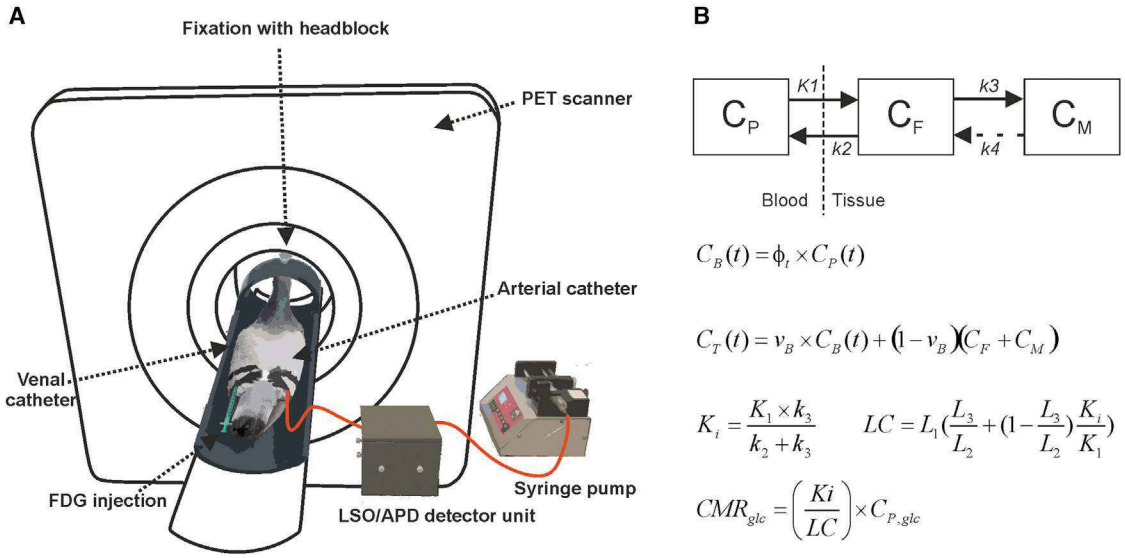

Figure 1. Overview of the experimental set-up and two-tissue compartment model

(A) Schematic representation of an awake scanning set-up following an intravenous (i.v.) [^{18}F]FDG injection. The pigeon was fixed in a holding tube secured via an implanted headblock. [^{18}F]FDG was injected via a catheter in the brachial vein, and arterial blood was sampled via a catheter in the brachial artery. During the first 2 min, blood was sampled automatically with a syringe pump set to a pulling speed of 1 ml/min, and plasma radioactivity was measured online via a lutetium oxyorthosilicate/avalanche photodiodes (LSO/APD) detector unit.

(B) [^{18}F]FDG kinetics were determined using a two-tissue compartment model (top). It assumes two compartments that represent blood and tissue and four kinetic rate constants. The [^{18}F]FDG first accumulates in the plasma (C_P) and is then transferred into the tissue (K_1) where it resides as free [^{18}F]FDG (C_F). Next, it is either transported back into the blood stream (k_2), or it enters the metabolic cycle and is phosphorylated (k_3) into metabolized [^{18}F]FDG (C_M). From here, it can be de-phosphorylated (k_4) back into free [^{18}F]FDG. The concentration of [^{18}F]FDG in the tissue (C_T) can be described as the fractional blood volume (v_B) multiplied by the concentration in blood (C_B, calculated from plasma activity times plasma fraction), added with the fractional tissue volume (1 $-v_B$) multiplied by the concentration of free [^{18}F]FDG plus metabolized [^{18}F]FDG. The exact concentrations of free and metabolized [^{18}F]FDG cannot be determined directly. Instead, final glucose metabolism (CMR_{glc}) can be calculated from established kinetic rate constants, the measured post-scan venous glucose plasma levels ($C_{P,glc}$), and the difference in kinetics of [^{18}F]FDG and glucose metabolism as described by the lumped constant (LC).

plasma glucose levels (see STAR methods for details of the mathematical modeling).

[^{18}F]FDG distribution and uptake in the pigeon brain

Quantitative CMR_{glc} assessment was executed in 4 awake and 6 isoflurane-anesthetized pigeons. The injected dose of [^{18}F]FDG did not differ between the awake and anesthetized group ($t(8) = -0.255$, $p = 0.805$) and ranged from 53.9 to 70.4 MBq, with an average of 65.39 ± 4.70 MBq. Post-scan venous glucose levels (12.40 ± 1.68 mmol/L) were within the normoglycemic range for birds.[15] Raw parametric images showed that [^{18}F]FDG was taken up and distributed throughout the entire brain in both the awake (Figure 2A) and anesthetized state (Figure S1). To determine the AIF, continuous arterial blood was automatically sampled during the first 2 min and manually sampled at specific time intervals for the rest of the scan (Figure 2B). The modeling approach showed a good fit between the TAC and fitted TAC (Figure 2C). The residual differences (Figure 2C, inset) at almost all points were below ± 5% (see Figure S2 for the arterial input function, TAC, and fitted TAC of all individuals in both the awake and anesthetized state).

Assessment of a pigeon-specific lumped constant

The lumped constant (LC) describes differences in the kinetics of glucose and [^{18}F]FDG. It is a crucial variable in the model, and some variation is present in the mammalian literature.[16] This variation has been ascribed to methodological differences, specificities of species, or disease state.[17,18] Following Backes et al.,[12] here we employed a model-dependent method in which the local LC is calculated from the rate constants of [^{18}F]FDG. It elaborates on the idea that disentangling transport and phosphorylation, which are lumped in the LC is more accurate than the application of a whole-brain LC.[18] The LC can be decomposed into the underlying processes it describes, i.e., transport and phosphorylation, and the difference in efficiencies between [^{18}F]FDG and glucose of these processes can be broken up into the following: $L_1 = K_{1,FDG}/K_{1,glc}$, $L_2 = k_{2,FDG}/k_{2,glc}$, and $L_3 = k_{3,FDG}/k_{3,glc}$. In humans and rats, the values of the separate ratios were found to be conserved across species and have been estimated at $L_1 = 1.48$, $L_2 = 1.48$, and $L_3 = 0.37$.[13,14] The local LC in each individual pigeon can then be calculated as a function of the pigeon-specific local kinetic rate constants (see Figure 1B for the LC formula). We found that the LC values did not differ between the awake and anesthetized group ($t(7) = 1.471$, $p = 0.185$) and averaged 0.69 ± 0.037. This value is at the high end of the range employed in mammalian studies (0.45–0.7[16,18,19]).

Possible caveats of this approach

This approach does assume that the kinetic rate differences of glucose and [^{18}F]FDG for transport (L_1, L_2) and phosphorylation (L_3) are comparable between pigeons and rats/humans. An empirical assessment of these variables would in theory be

Please cite this article in press as: von Eugen et al., Avian neurons consume three times less glucose than mammalian neurons, Current Biology (2022), https://doi.org/10.1016/j.cub.2022.07.070

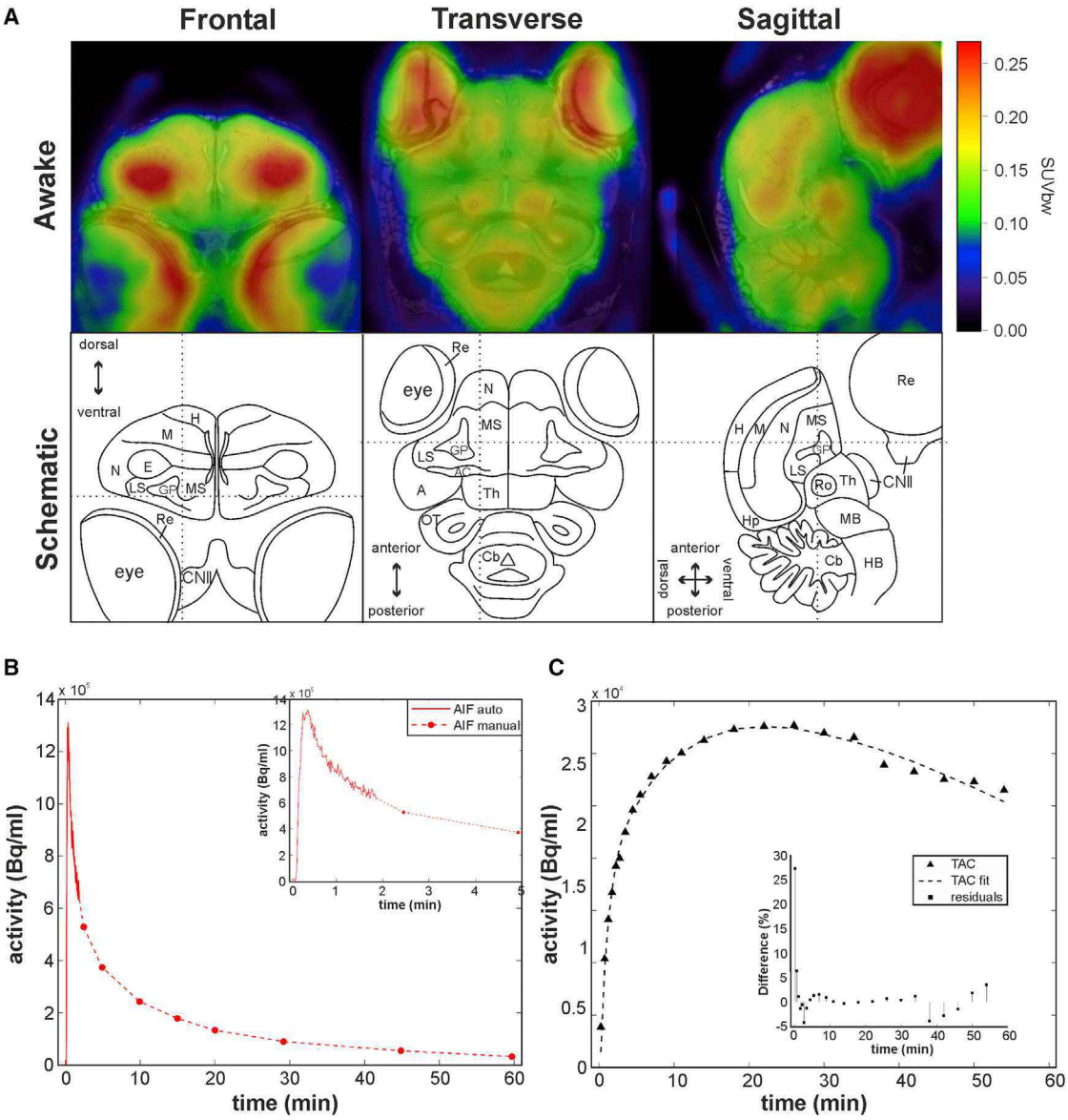

Figure 2. Example of [^{18}F]FDG distribution in the awake brain, arterial input function, and model fit

(A) Cerebral [^{18}F]FDG activity fused with a structural magnetic resonance (MR)-image in the awake state with schematic overview of the brain. Dotted lines indicate the exact plane in frontal (left), transversal (middle), and sagittal (right) sections. The heat map represents standardized uptake value, corrected for body weight (SUVbw = image activity [Bq/ml] × bw [g] / injected dose [Bq]), with red indicating high and blue low levels of uptake. The distribution in the awake state indicates relatively higher levels in the pecten oculi (not visible in these sections) and retina, as well as entopallium, which is one of the two primary visual pallial areas in birds.

See Figure S1 for the anesthetized state and Figure S3 for average CMR_{glc} values for forebrain, cerebellum, and the rest of brain in both awake and anesthetized state.

(B) Representative arterial input function (AIF) in the awake state. Following an intravenous (i.v.) injection, the AIF shows an initial sharp peak captured by the automatic sampling device (AIF auto). The peak quickly drops and slopes off to a plateau, captured by manual sampling at later time points (AIF manual). The inset depicts the initial 5 min.

(C) Example of a model fit in the awake state. The two-tissue compartment model fit (dotted line) corresponds well to the time-activity curve of the whole brain (black triangles). The inset depicts residual differences in percentage, where, except for the first time point (~27%), all fits differ less than ± 5%.

See Figure S2 for the AIF, TAC, model fit and residuals for all pigeons. A, arcopallium; AC, anterior commissure; BS, brainstem; CN II, second cranial nerve (optic nerve); Cb, cerebellum; E, entopallium; GP, globus pallidus; H, hyperpallium; HB, hindbrain; Hp, hippocampus; LS, lateral striatum; M, mesopallium; MB, midbrain; MS, medial striatum; N, nidopallium; OT, optic tectum; Re, retina; Ro, nucleus rotundus; RH, right hemisphere; Th, rest of thalamus.

Please cite this article in press as: von Eugen et al., Avian neurons consume three times less glucose than mammalian neurons, Current Biology (2022), https://doi.org/10.1016/j.cub.2022.07.070

Table 1. K-parameters, LC, and CMR_{glc} for whole brain per subject

Pigeon ID	K_1 (1/min)	k_2 (1/min)	k_3 (1/min)	k_4 (1/min)	K_i (mL/g/min)	LC	CMR_{glc} (μmol/100 g/min)
Awake							
752	0.063	0.16	0.061	0.012	0.018	0.69	29.21
886	0.058	0.16	0.062	0.012	0.016	0.70	26.69
920	0.061	0.15	0.062	0.012	0.017	0.70	25.51
986	0.055	0.15	0.072	0.013	0.018	0.75	27.74
Mean ± SD							
–	0.059 ± 0.0036	0.15 ± 0.0046	0.065 ± 0.0050	0.012 ± 0.00026	0.018 ± 0.00078	0.71 ± 0.025	27.29 ± 1.57
Anesthetized							
146	0.045	0.16	0.045	0.017	0.010	0.62	19.22
232	0.040	0.14	0.059	0.012	0.012	0.71	23.67
536	0.049	0.15	0.061	0.012	0.014	0.70	30.76
590	0.056	0.15	0.045	0.017	0.012	0.64	25.10
645	0.033	0.11	0.080	0.030	0.014	0.86*	23.01
877	0.039	0.15	0.061	0.012	0.011	0.70	17.11
Mean ± SD							
–	0.044 ± 0.0083	0.14 ± 0.019	0.059 ± 0.013	0.017 ± 0.0070	0.012 ± 0.0017	0.68 ± 0.040	23.15 ± 4.77

The 2-compartment model generates four kinetic rate constants (K_1, k_2, k_3, and k_4) that describe the metabolic process of [^{18}F]FDG. K_i describes the net influx of [^{18}F]FDG. The lumped constant (LC) describes the difference in kinetics of [^{18}F]FDG and glucose metabolism. The outlier 645 (*) of the anesthetized group was excluded from further analysis of the LC. The final cerebral metabolic rate of glucose (CMR_{glc}) can be calculated from the kinetic rate constants. See Table S1 for an overview of K-parameters and CMR_{glc} calculated with varying blood volume percentage of the brain.

possible,[11] but it is not trivial and possibly not even feasible in the used model organism due to its specific physiology. Thus, we decided to not perform such an assessment, since this was outside the experimental scope of our study, and there is a good body of literature supporting the assumption that L_1–L_3 are invariant between species. In the mammalian nervous system, glucose is primarily transported by glucose transporter proteins (GLUT) 1 and 3. Likewise, high levels of mRNA and protein expression of GLUT1 and GLUT3 were found in the brains of different bird species,[20,21] with a high degree of similarity in genetic and amino acid sequences.[21] Furthermore, even though human GLUT1 and GLUT3 differ highly in structure and glucose affinity, kinetic rate differences between glucose and [^{18}F]FDG transport (L_1, L_2) are still identical for both transporters, strongly supporting the claim of a fixed kinetic rate difference.[22]

The same holds true for glucose phosphorylation and the related kinetic rate difference L_3. In the mammalian brain, glucose is phosphorylated to glucose-6-phosphate by hexokinase 1. A comparison of pigeons, chickens, and rats demonstrated similar activity and specificity levels of hexokinase 1,[23] and a sequence analysis with UniProt revealed 88% similarity between the human and avian hexokinase 1. This indicates a similar if not identical processing of glucose in birds and mammals by hexokinase 1, and it is very unlikely that this differs for [^{18}F]FDG. However, when interpreting our data, it should be kept in mind that we cannot fully exclude differences in L_1–L_3 between avian and mammalian species, which could, in theory, affect the data pattern.

Kinetic rate constants and CMR_{glc}

Kinetic modeling derived four kinetic rate constants (Table 1). The local glucose consumption rate, expressed as CMR_{glc}, was calculated from the metabolic rate constant K_i divided by the local LC and multiplied by the post-scan venous plasma glucose level. There was no significant difference between the awake and anesthetized state for whole brain CMR_{glc}, $t(8) = 1.648$, $p = 0.069$, with 27.29 ± 1.57 μmol/100 g/min in the awake state compared to 23.15 ± 4.77 μmol/100 g/min in the anesthetized state. This was surprising since in mammals, anesthesia has been found to have a diminishing effect on cerebral glucose consumption.[8] One explanation could be that in these mammalian studies, only parts of the brain were analyzed as opposed to the whole brain. Indeed, when we analyzed the CMR_{glc} of separate brain regions, significant effects of anesthesia were found (Figure S3). The mass-specific CMR_{glc} is comparable to what has been found in humans (26.08 ± 1.78 μmol/100 g/min,[19,24,25]) and almost three times as low compared to the similarly body- and brain-sized rat (68.00 ± 4.00 μmol/100 g/min,[26–28]).

The neuronal energy budget in the awake pigeon

To relate the calculated CMR_{glc} of the pigeon to the mammalian neuronal energy budget, glucose consumption of the whole brain in the awake state was divided by the known number of neurons in the pigeon brain.[7] Of course, the brain does not only consist of neurons but is a mosaic of neuronal and non-neuronal cell types that require energy in the form of glucose for both active processes and housekeeping costs.[4,29–31] In our analysis, we only included neurons, since most of the cerebral energy budget (70%–80%) has been estimated to support neuronal signaling costs.[4,29,30] The determined budget can thus be understood as the glucose needed to support one neuron either directly or indirectly.[3] This large contribution became evident when we estimated the glucose budget over both neurons and glial cells, revealing a highly similar pattern (Figure S4). We compared our

Please cite this article in press as: von Eugen et al., Avian neurons consume three times less glucose than mammalian neurons, Current Biology (2022), https://doi.org/10.1016/j.cub.2022.07.070

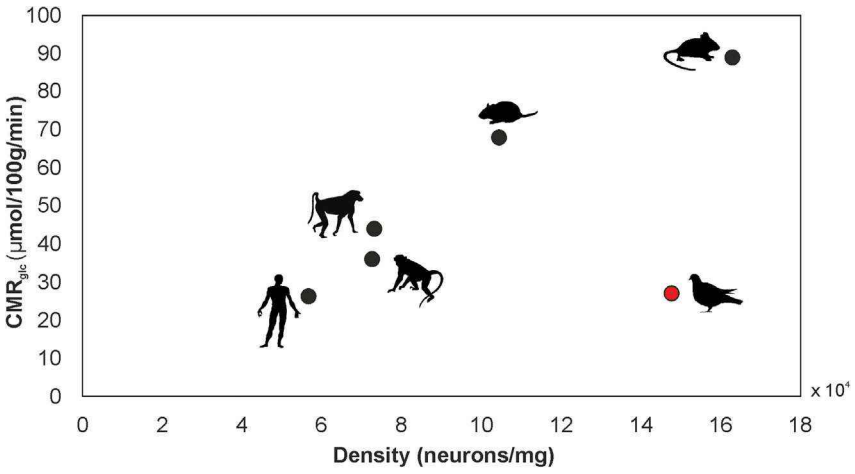

Figure 3. Scaling of mean-specific CMR_{glc} and neuron density in the whole brain across species

Neuronal densities per mg are plotted on the x axis and µmol glucose consumption per 100 g per minute on the y axis, thus the graph represents CMR_{glc} per neuron across different mammalian species and the pigeon. All mammalian species fall on the same regression line that can be described by a linear function $5.76 \times 10^{-6} X + 5.62 \times 10^{-9}$ ($R^2 = 0.949$, $p = 0.005$).[3] This corresponds to an average CMR_{glc} per neuron of $5.79 \times 10^{-9} \pm 0.76 \times 10^{-9}$. In contrast, in the pigeon, a neuron consumes on average $1.86 \times 10^{-9} \pm 0.2 \times 10^{-9}$, which is 3.11 times lower than the average mammalian neuron. See Figure S4 for CMR_{glc} per cell (neuronal and glial cells combined) in the whole brain across species. See Table S2 for neuronal densities, $CMR_{glc,}$ and the neuronal energy budget per species. CMR_{glc} data were available for mouse,[34] rat,[26–28] monkey,[35] baboon,[36] and human[19,24,25] and combined with estimated neuron numbers.[37] Neuron numbers in the pigeon come from Olkowics et al.[7] Silhouettes were obtained from http://phylopic.org under public license.

findings to mammalian data that were either collected with the same [^{18}F]FDG-PET method as we employed or by autoradiography using the radioactively labeled glucose analog 2-deoxy-D-14C-glucose ([^{14}C]DG). Since the CMR_{glc} in both approaches was modeled using the same two-tissue compartment model, and several studies found no or only minor differences between the two methods,[32,33] we assume that both datasets are directly comparable to our findings.

Since we found that pigeon brain tissue requires 27.29 ± 1.57 µmol glucose per 100 g per min, this translates as $1.86 \times 10^{-9} \pm 0.2 \times 10^{-9}$ µmol glucose per neuron per minute. This is an astonishing 3.11 times lower than the mammalian whole-brain neuronal energy budget of $5.79 \times 10^{-9} \pm 0.76 \times 10^{-9}$ µmol glucose per neuron per minute[3] (Figure 3). This finding explains how pigeons, and possibly other avian species, are able to sustain almost twice as many neurons as a similarly sized mammal, without the associated metabolic costs. What could be the underlying mechanistic explanation for this reduction in the energy budget?

Potential factors explaining the reduced neuronal energy budget

There is ample evidence that any increase in size of parts of or the whole nervous system evolved under a selection pressure to reduce energy consumption.[6,38] This can be achieved by either reducing the costs of signaling itself, with alterations in the biophysical properties of cells and circuits, or with alternative coding strategies.[39] Understanding how energy efficiency is obtained within the brain starts with collecting detailed neuroanatomical and neurophysiological data such as neuron size, firing rates, ion channel kinetics, membrane capacitance, etc. Based on these data, computational models can test theoretical predictions of optimal energy efficiency under specific conditions.[39] Currently, most of the crucial data are lacking for birds. This highly complicates identifying any underlying mechanism for the low neuronal energy costs. Based on what is known, we can identify two potential contributing biophysical properties that differ in birds compared with mammals: namely, neuron size and brain temperature.

Cell size is a key factor in the metabolism of any neuron and correlates positively with energy consumption.[30,40] Though no systematic survey has ever been conducted in birds, there is support for the idea that the average avian neuron size is smaller than in mammals. As mentioned above, neuron densities in the avian brain are much higher compared to similarly sized mammals, and this likely translates into small neuronal sizes and short interneural distances.[7,41] Indeed, a mathematical approach demonstrated that neuron and non-neuronal cell density could be used as an indicator of cell size, where higher density corresponds to smaller neuron sizes.[42] Moreover, from comparison between the macaque and mouse, it is known that some specific neuron types indeed scale positively with increasing brain size.[43] A smaller neuron is more energy efficient in a variety of ways.[44,45] For example, in line with the reduced membrane surface area and cytoplasmic volume, smaller neurons accommodate fewer receptors, ion channels, and mitochondria. They are also characterized by a lower membrane capacitance. Lastly, the overall lower number of components translates into reduced maintenance and housekeeping costs. Thus, smaller neuron sizes could explain, at least in part, the lower metabolic costs we observe in the pigeon brain.

Next to neuron size, another stark difference between birds and mammals is the higher body, and thus brain, temperature in birds.[46] In pigeons, the core brain temperature measures 40°C–42°C[47] compared with 36ºC–37ºC in the rat brain.[48] The effect of temperature on behavior and neural activity is a widespread phenomenon, and it influences multiple cellular components and dynamics, including the resting membrane potential, generation of action potentials, synaptic transmission, and axon conduction velocity.[49] For example, increases in temperature of 1.5 degrees have been recorded in rat hippocampus during active exploration, in concordance with changes in the waveform of action potentials.[50] These interactions have also been found in birds. In zebra finches, the cooling of specific song-related brain nuclei had a causal decreasing effect on song tempo.[51] This is not just an effect of experimental manipulation, because zebra finches show natural temperature fluctuations related to a diurnal cycle and social context; in correlation to

Please cite this article in press as: von Eugen et al., Avian neurons consume three times less glucose than mammalian neurons, Current Biology (2022), https://doi.org/10.1016/j.cub.2022.07.070

either a decrease or increase in brain temperature, the song tempo decreased or increased, respectively.[52] At the basis of many of these processes is the direct effect of temperature on ion channel kinetics, maximum conductance, and gating kinetics.[53] The most prominent example of this effect is its influence on the time of overlap between Na^+ and K^+ currents that flow across the membrane during an action potential. Time of overlap and costs are positively correlated, since higher numbers of ions need to be pumped across the membrane by the Na^+/K^+-ATPase after the action potential. Higher temperatures were found to exponentially and strongly decrease the time constants of Na^+ and K^+ channel activation and inactivation, thereby lowering the energy costs.[54] This type of modulation of ion channel kinetics not only reduces costs of individual neurons but also seems to improve signal transmission. This was demonstrated in the swordfish (*Xiphias gladius*), where regional warming of the eye and brain improved temporal resolution of visual processing by a factor of ten.[55] Thus, the higher brain temperature present in birds could contribute to reducing energy consumption of neurons by both making ion channel kinetics more efficient and improving information rates.

Evolutionary perspective

It is important to keep in mind that what is "economical" compared to a mammal can still be costly for a bird. Indeed, across different bird species, we observe many examples indicating that neurons are not a free-for-all commodity. This is clearly apparent in songbirds, which demonstrate some of the most impressive types of neuroplasticity among adult vertebrates. The most extreme example comes from the spotted towhee (*Pipilo maculatus*), whose HVC (a song nucleus important for learning of song) in males can increase 300% in size during a breeding season to facilitate complex song repertoires to attract mates and defend territory.[56] Of course, it is unlikely that any organism wastes neuron numbers or other costly tissue.[57] These extreme examples of neuroplasticity do show that avian species are under particularly high pressure to reduce (cerebral) energy consumption. In addition, the higher body temperature and costly capacity of flight might also be crucial contributing factors.[46,58]

As mentioned, despite this extreme pressure, birds attain higher neuron numbers compared to similarly sized mammalian species;[7] like mammals,[59] these numbers positively correlate with cognitive performance.[60] Our findings from pigeons suggest that the ceiling on neuron numbers might be raised by attaining a 3-fold lower neuronal energy budget. Future studies will have to verify whether this is a class-wide phenomenon, but the high neuron densities observed across almost all avian species studied so far can be taken as a first indicator that this is the case.[7] Importantly, the lower budget does not seem to compromise neuronal computations, since birds are considered perceptually and cognitively on par with mammals.[10] The last common ancestor of birds and mammals existed approximately 312 mya,[61] and in the long parallel evolution of both lineages, birds ended up with tiny brains comprising high numbers of small neurons organized in a distinct cerebral layout[7,10] and situated in a warmer physiology.[46] The combined effect of these distinct elements on neuronal dynamics generated a possible advantage in neuronal processing of information at a higher efficiency: cheap neurons with advanced processing capacity.

STAR★METHODS

Detailed methods are provided in the online version of this paper and include the following:

- KEY RESOURCES TABLE
- RESOURCE AVAILABILITY
  - Lead contact
  - Materials availability
  - Data and code availability
- EXPERIMENTAL MODEL AND SUBJECT DETAILS
- METHOD DETAILS
  - PET data acquisition
  - Validation of handheld glucometer
  - Input function
  - Image processing
  - Kinetic modeling
- QUANTIFICATION AND STATISTICAL ANALYSIS

SUPPLEMENTAL INFORMATION

Supplemental information can be found online at https://doi.org/10.1016/j.cub.2022.07.070.

ACKNOWLEDGMENTS

The authors thank Lukas Vieth, Roland Pusch, and Lynn Wenke for laboratory assistance. Furthermore, we would like to thank Suzana Herculano-Houzel for her theoretical input. Supported by the Deutsche Forschungsgemeinschaft through Gu 227/16-1 and Gu 227/21-1.

AUTHOR CONTRIBUTIONS

F.S., O.G., and H.E. conceived the experiments; F.S., K.v.E., and H.E. performed the experiments; H.B., H.E., and K.v.E. analyzed the data; K.v.E. wrote the original draft; A.D., B.N., F.S., O.G., H.E., and H.B. reviewed and edited the draft; F.S. and O.G. secured funding.

DECLARATION OF INTERESTS

The authors declare no competing interests.

Received: October 19, 2021
Revised: April 11, 2022
Accepted: July 26, 2022
Published: September 8, 2022

REFERENCES

1. Mink, J.W., Blumenschine, R.J., and Adams, D.B. (1981). Ratio of central nervous system to body metabolism in vertebrates: Its constancy and functional basis. Am. J. Physiol. *241*, 203–212.
2. Dienel, G.A. (2019). Brain glucose metabolism: Integration of energetics with function. Physiol. Rev. *99*, 949–1045.
3. Herculano-Houzel, S. (2011). Scaling of brain metabolism with a fixed energy budget per neuron: Implications for neuronal activity, plasticity and evolution. PLoS One *6*, e17514.
4. Hyder, F., Rothman, D.L., and Bennett, M.R. (2013). Cortical energy demands of signaling and nonsignaling components in brain are conserved across mammalian species and activity levels. Proc. Natl. Acad. Sci. USA. *110*, 3549–3554.
5. Roth, G., and Dicke, U. (2005). Evolution of the brain and intelligence. Trends Cognit. Sci. *9*, 250–257.

6. Niven, J.E., and Laughlin, S.B. (2008). Energy limitation as a selective pressure on the evolution of sensory systems. J. Exp. Biol. *211*, 1792–1804.
7. Olkowicz, S., Kocourek, M., Lučan, R.K., Porteš, M., Fitch, W.T., Herculano-Houzel, S., Němec, P., Lučan, R.K., Porteš, M., Fitch, W.T., et al. (2016). Birds have primate-like numbers of neurons in the forebrain. Proc. Natl. Acad. Sci. USA. *113*, 7255–7260.
8. Kuntner, C. (2014). Kinetic modeling in pre-clinical positron emission tomography. Z. Med. Phys. *24*, 274–285.
9. Karbowski, J. (2007). Global and regional brain metabolic scaling and its functional consequences. BMC Biol. *5*, 18–21.
10. Güntürkün, O., and Bugnyar, T. (2016). Cognition without Cortex. Trends Cognit. Sci. *20*, 291–303.
11. Sokoloff, L., Reivich, M., Kennedy, C., Des Rosiers, M.H., Patlak, C.S., Pettigrew, K.D., Sakurada, O., and Shinohara, M. (1977). THe [14C]deoxyglucose method for the measurement of local cerebral glucose utilization: theroy, procedure, and normal values in the conscious and anesthetized albino rat. J. Neurochem. *28*, 897–916.
12. Backes, H., Walberer, M., Endepols, H., Neumaier, B., Graf, R., Wienhard, K., and Mies, G. (2011). Whiskers Area as Extracerebral Reference Tissue for Quantification of Rat Brain Metabolism Using 18F-FDG PET: Application to Focal Cerebral Ischemia. J. Nucl. Med. *52*, 1252–1260.
13. Hasselbalch, S.G., Madsen, P.L., Knudsen, G.M., Holm, S., and Paulson, O.B. (1998). Calculation of the FDG lumped constant by simultaneous measurements of global glucose and FDG metabolism in humans. J. Cerebr. Blood Flow Metabol. *18*, 154–160.
14. Hasselbalch, S.G., Knudsen, G.M., Holm, S., Hageman, L.P., Capaldo, B., and Paulson, O.B. (1996). Transport of D-glucose and 2-fluorodeoxyglucose across the blood-brain barrier in humans. J. Cerebr. Blood Flow Metabol. *16*, 659–666.
15. Scanes, C.G. (2015). Carbohydrate Metabolism. In Sturkie's Avian Physiology, Sixth Edition (Elsevier Inc.), pp. 421–441.
16. Alf, M.F., Duarte, J.M.N., Lei, H., Krämer, S.D., Mlynarik, V., Schibli, R., and Gruetter, R. (2014). MRS glucose mapping and PET joining forces: re-evaluation of the lumped constant in the rat brain under isoflurane anaesthesia. J. Neurochem. *129*, 672–682.
17. Krohn, K.A., Muzi, M., and Spence, A.M. (2007). What Is in a Number? The FDG Lumped Constant in the Rat Brain. J. Nucl. Med. *48*, 5–7.
18. Kuwabara, H., Evans, A.C., and Gjedde, A. (1990). Michaelis-Menten constraints improved cerebral glucose metabolism and regional lumped constant measurements with [18F]fluorodeoxyglucose. J. Cerebr. Blood Flow Metabol. *10*, 180–189.
19. Sundar, L.K., Muzik, O., Rischka, L., Hahn, A., Rausch, I., Lanzenberger, R., Hienert, M., Klebermass, E.M., Füchsel, F.G., Hacker, M., et al. (2019). Towards quantitative [18F]FDG-PET/MRI of the brain: Automated MR-driven calculation of an image-derived input function for the non-invasive determination of cerebral glucose metabolic rates. J. Cerebr. Blood Flow Metabol. *39*, 1516–1530.
20. Braun, E.J., and Sweazea, K.L. (2008). Glucose regulation in birds. Comp. Biochem. Physiol. B Biochem. Mol. Biol. *151*, 1–9.
21. Welch, K.C., Allalou, A., Sehgal, P., Cheng, J., and Ashok, A. (2013). Glucose Transporter Expression in an Avian Nectarivore: The Ruby-Throated Hummingbird (Archilochus colubris). PLoS One *8*, e77003.
22. Custódio, T.F., Paulsen, P.A., Frain, K.M., and Pedersen, B.P. (2021). Structural comparison of GLUT1 to GLUT3 reveal transport regulation mechanism in sugar porter family. Life Sci. Alliance *4*, e202000858.
23. Sugden, P.H., and Newsholme, E.A. (1973). Activities of hexokinase, phosphofructokinase, 3-oxo acid coenzyme A-transferase and acetoacetyl-coenzyme A thiolase in nervous tissue from vertebrates and invertebrates. Biochem. J. *134*, 97–101.
24. Sari, H., Erlandsson, K., Law, I., Larsson, H.B., Ourselin, S., Arridge, S., Atkinson, D., and Hutton, B.F. (2017). Estimation of an image derived input function with MR-defined carotid arteries in FDG-PET human studies using a novel partial volume correction method. J. Cerebr. Blood Flow Metabol. *37*, 1398–1409.
25. Huisman, M.C., van Golen, L.W., Hoetjes, N.J., Greuter, H.N., Schober, P., Ijzerman, R.G., Diamant, M., and Lammertsma, A.A. (2012). Cerebral blood flow and glucose metabolism in healthy volunteers measured using a high-resolution PET scanner. EJNMMI Res. *2*, 63–69.
26. Nehlig, A., de Vasconcelos, A.P., and Boyet, S. (1988). Quantitative autoradiographic measurement of local cerebral glucose utilization in freely moving rats during postnatal development. J. Neurosci. *8*, 2321–2333.
27. Waschke, K., Schröck, H., Albrecht, D.M., Van Ackern, K., and Kuschinsky, W. (1993). Local cerebral blood flow and glucose utilization after blood exchange with a hemoglobin-based O2carrier in conscious rats. Am. J. Physiol. *265*, H1243–H1248.
28. Levant, B., and Pazdernik, T.L. (2004). Differential effects of ibogaine on local cerebral glucose utilization in drug-naive and morphine-dependent rats. Brain Res. *1003*, 159–167.
29. Yu, Y., Herman, P., Rothman, D.L., Agarwal, D., and Hyder, F. (2018). Evaluating the gray and white matter energy budgets of human brain function. J. Cerebr. Blood Flow Metabol. *38*, 1339–1353.
30. Howarth, C., Gleeson, P., and Attwell, D. (2012). Updated energy budgets for neural computation in the neocortex and cerebellum. J. Cerebr. Blood Flow Metabol. *32*, 1222–1232.
31. Engl, E., and Attwell, D. (2015). Non-signalling energy use in the brain. J. Physiol. *593*, 3417–3429.
32. Reivich, M., Alavi, A., Wolf, A., Fowler, J., Russell, J., Arnett, C., MacGregor, R.R., Shiue, C.Y., Atkins, H., and Anand, A. (1985). Glucose metabolic rate kinetic model parameter determination in humans: The lumped constants and rate constants for [18F]fluorodeoxyglucose and [11C]deoxyglucose. J. Cerebr. Blood Flow Metabol. *5*, 179–192.
33. Toyama, H., Ichise, M., Liow, J.-S., Modell, K.J., Vines, D.C., Esaki, T., Cook, M., Seidel, J., Sokoloff, L., Green, M.V., and Innis, R.B. (2004). Absolute quantification of regional cerebral glucose utilization in mice by 18F-FDG small animal PET scanning and 2-14C-DG autoradiography - PubMed. J. Nucl. Med. *45*, 1398–1405.
34. Bouilleret, V., Boyet, S., Marescaux, C., and Nehlig, A. (2000). Mapping of the progressive metabolic changes occurring during the development of hippocampal sclerosis in a model of mesial temporal lobe epilepsy. Brain Res. *852*, 255–262.
35. Kennedy, C., Sakurada, O., Shinohara, M., Jehle, J., and Sokoloff, L. (1978). Local cerebral glucose utilization in the normal conscious macaque monkey. Ann. Neurol. *4*, 293–301.
36. Meguro, K., Blaizot, X., Kondoh, Y., Le Mestric, C., Baron, J.C., and Chavoix, C. (1999). Neocortical and hippocampal glucose hypometabolism following neurotoxic lesions of the entorhinal and perirhinal cortices in the non-human primate as shown by PET. Implications for Alzheimer's disease. Brain. *122*, 1519–1531.
37. Herculano-Houzel, S., Catania, K., Manger, P.R., and Kaas, J.H. (2015). Mammalian Brains Are Made of These: A Dataset of the Numbers and Densities of Neuronal and Nonneuronal Cells in the Brain of Glires, Primates, Scandentia, Eulipotyphlans, Afrotherians and Artiodactyls, and Their Relationship with Body Mass. Brain Behav. Evol. *86*, 145–163.
38. Yu, L., and Yu, Y. (2017). Energy-efficient neural information processing in individual neurons and neuronal networks. J. Neurosci. Res. *95*, 2253–2266.
39. Niven, J.E. (2016). Neuronal energy consumption: biophysics, efficiency and evolution. Curr. Opin. Neurobiol. *41*, 129–135.
40. Niven, J.E., Anderson, J.C., and Laughlin, S.B. (2007). Fly Photoreceptors Demonstrate Energy-Information Trade-Offs in Neural Coding. PLoS Biol. *5*, e116.
41. Dicke, U., and Roth, G. (2016). Neuronal factors determining high intelligence. Philos. Trans. R. Soc. Lond. B Biol. Sci. *371*, 20150180.
42. Mota, B., and Herculano-Houzel, S. (2014). All brains are made of this: a fundamental building block of brain matter with matching neuronal and glial masses. Front. Neuroanat. *8*, 127.

43. Gilman, J.P., Medalla, M., and Luebke, J.I. (2017). Area-Specific Features of Pyramidal Neurons-a Comparative Study in Mouse and Rhesus Monkey. Cereb. Cortex *27*, 2078–2094.

44. Sengupta, B., Faisal, A.A., Laughlin, S.B., and Niven, J.E. (2013). The effect of cell size and channel density on neuronal information encoding and energy efficiency. J. Cerebr. Blood Flow Metabol. *33*, 1465–1473.

45. Niven, J.E., and Farris, S.M. (2012). Miniaturization of Nervous Systems and Neurons. Curr. Biol. *22*, R323–R329.

46. Prinzinger, R., Preßmar, A., and Schleucher, E. (1991). Body temperature in birds. Comp. Biochem. Physiol. Physiol. *99*, 499–506.

47. Kilgore, D.L., Bernstein, M.H., and Hudson, D.M. (1976). Brain temperatures in birds. J. Comp. Physiol. *110*, 209–215.

48. Alföldi, P., Rubicsek, G., Cserni, G., and Obál, F., Jr. (1990). Brain and core temperatures and peripheral vasomotion during sleep and wakefulness at various ambient temperatures in the rat. Pflugers Arch. *417*, 336–341.

49. Wang, H., Kim, M., Normoyle, K.P., and Llano, D. (2016). Thermal Regulation of the Brain—An Anatomical and Physiological Review for Clinical Neuroscientists. Front. Neurosci. *9*, 528.

50. Andersen, P., and Moser, E.I. (1995). Brain temperature and hippocampal function. Hippocampus *5*, 491–498.

51. Andalman, A.S., Foerster, J.N., and Fee, M.S. (2011). Control of Vocal and Respiratory Patterns in Birdsong: Dissection of Forebrain and Brainstem Mechanisms Using Temperature. PLoS One *6*, e25461.

52. Aronov, D., and Fee, M.S. (2012). Natural Changes in Brain Temperature Underlie Variations in Song Tempo during a Mating Behavior. PLoS One *7*, e47856.

53. Georgiev, G., Valova, I., Gueorguieva, N., and Brady, D. (2014). Simulating Influence of Channel Kinetics and Temperature on Hodgkin-Huxley Threshold Dynamics. Procedia Comput. Sci. *36*, 464–469.

54. Yu, Y., Hill, A.P., and McCormick, D.A. (2012). Warm body temperature facilitates energy efficient cortical action potentials. PLoS Comput. Biol. *8*, 1002456.

55. Fritsches, K.A., Brill, R.W., and Warrant, E.J. (2005). Warm Eyes Provide Superior Vision in Swordfishes. Curr. Biol. *15*, 55–58.

56. Tramontin, A.D., and Brenowitz, E.A. (2000). Seasonal plasticity in the adult brain. Trends Neurosci. *23*, 251–258.

57. Wilkens, H., and Strecker, U. (2017). The Role of Rudimentation in Evolution. In Evolution in the Dark (Berlin, Heidelberg: Springer), pp. 3–12.

58. Schmidt-Nielsen, K. (1972). Locomotion: Energy cost of swimming, flying, and running. Science *177*, 222–228.

59. Herculano-Houzel, S., Manger, P.R., and Kaas, J.H. (2014). Brain scaling in mammalian evolution as a consequence of concerted and mosaic changes in numbers of neurons and average neuronal cell size. Front. Neuroanat. *8*, 1–28.

60. Ströckens, F., Neves, K., Kirchem, S., Schwab, C., Herculano-Houzel, S., and Güntürkün, O. (2022). High associative neuron numbers could drive cognitive performance in corvid species. J. Comp. Neurol. *530*, 1588–1605.

61. Benton, M.J., and Donoghue, P.C.J. (2006). Paleontological Evidence to Date the Tree of Life. Mol. Biol. Evol. *24*, 26–53.

62. Breuer, J., Grazioso, R., Zhang, N., Schmand, M., and Wienhard, K. (2010). Evaluation of an MR-compatible blood sampler for PET. Phys. Med. Biol. *55*, 5883–5893.

63. Behroozi, M., Helluy, X., Ströckens, F., Gao, M., Pusch, R., Tabrik, S., Tegenthoff, M., Otto, T., Axmacher, N., Kumsta, R., et al. (2020). Event-related functional MRI of awake behaving pigeons at 7T. Nat. Commun. *11*, 4715.

64. Qi, J., Leahy, R.M., Cherry, S.R., Chatziioannou, A., and Farquhar, T.H. (1998). High-resolution 3D Bayesian image reconstruction using the microPET small-animal scanner. Phys. Med. Biol. *43*, 1001–1013.

65. Vollmar, S., Hampl, J.A., Kracht, L., and Herholz, K. (2007). Integration of Functional Data (PET) into Brain Surgery Planning and Neuronavigation. Adv. Med. Eng. 98–103.

66. Heisey, S.R. (1968). Brain and choroid plexus blood volumes in vertebrates. Comp. Biochem. Physiol. *26*, 489–498.

Please cite this article in press as: von Eugen et al., Avian neurons consume three times less glucose than mammalian neurons, Current Biology (2022), https://doi.org/10.1016/j.cub.2022.07.070

STAR★METHODS

KEY RESOURCES TABLE

REAGENT or RESOURCE	SOURCE	IDENTIFIER
Chemicals, peptides, and recombinant proteins		
Ketamine hydrochloride/xylazine hydrochloride solution	Sigma-Aldrich	Cat# K113
Isoflurane	Piramal	https://www.piramalcriticalcare.com/german/products/fur-patienten/inhalative-anasthesie/isofluran/
2-[^{18}F]fluoro-2-deoxyglucose	Life Radiopharma f-con GmbH	https://www.liferadiopharma.com/
Critical commercial assays		
Glucose Colorimetric Assay Kit II	BioVision	Cat# K686
Experimental models: Organisms/strains		
Rock pigeon (*Columba livia*)	Local registered breeder	N/A
Software and algorithms		
VINCI version 4.90	Max Plank Institute for Metabolism Research	https://vinci.sf.mpg.de/
SPSS Statistics for Windows version 21.0	IBM	https://www.ibm.com/products/spss-statistics
Kinetic modeling algorithm (IDL, version 8.5.1, GNUPLOT, version 5.2, GCC compiler, version 7.5)	Backes et al.[12]	http://www.gnuplot.info/ https://gcc.gnu.org/
microPET Manager 2.5.0.0	Siemens Medical Solutions	N/A
ParaVision version 5.1	Bruker	https://www.bruker.com/en/services/software-downloads.html
Data acquisition software online blood sampler	Breuer et al.[62]	N/A

RESOURCE AVAILABILITY

Lead contact

Further information and requests for resources and reagents should be directed to and will be fulfilled by the lead contact, Felix Ströckens (felix.stroeckens@hhu.de).

Materials availability

This study did not generate new unique reagents.

Data and code availability

- All data reported in this paper will be shared by the lead contact upon request.
- This paper does not report original code.
- Any additional information required to reanalyze the data reported in this paper is available from the lead contact upon request.

EXPERIMENTAL MODEL AND SUBJECT DETAILS

The research proposal was reviewed and approved by the local animal ethics committee of Nordrhein-Westfalen Germany and in accordance with the German Animal Welfare law following the recommendations of the EU directive 86/609/EEC (permission number: 84-02-04-2017-A 160). For this study, 10 adult homing pigeons (*Columba livia*) of unknown sex were obtained from a local breeder. All pigeons were of a normal weight (464.80 ± 45.97 g). Pigeons were housed individually on a 12/12 h light/dark cycle. Food and water was provided *ad libitum*, except for an overnight fasting before surgeries to prevent aspirating food under anaesthesia and before scanning to facilitate similar blood glucose levels between individuals and states. To enable awake scanning, four individuals were implanted with a plastic head pedestal.[63] In short, under deep anaesthesia (ketamine/xylazine 0.12 ml/100 g body weight) an incision was made in the skin to lay bare the surface of the skull. Next, a small plastic head block was secured directly on the skull with dental cement and the skin was sutured. The head block was compatible with a custom-made holding tube to prevent any head motion in the scanner (Figure 1A). To reduce stress to a minimum, pigeons underwent a habituation procedure. One week prior to scanning, pigeons were habituated to the apparatus and procedure in a mock-PET environment for increasing time

Please cite this article in press as: von Eugen et al., Avian neurons consume three times less glucose than mammalian neurons, Current Biology (2022), https://doi.org/10.1016/j.cub.2022.07.070

lengths of 5, 10, 15, 30, and 45 minutes over five consecutive days. As demonstrated by Behroozi et al.,[63] this procedure reduces movement to a negligible minimum and eliminates all visible stress indicators. Namely, after a short increase, heart rate returned to normal levels within minutes and measurements of blood cortisol levels showed no increase after the habituation procedure. Therefore, we believe our results are minimally influenced by stress.

METHOD DETAILS

PET data acquisition

All PET scans were performed in a microPET Focus 220 PET scanner for small animals (CTI-Siemens, USA), see Figure 1A for experimental setup. Subjects (n = 10) were scanned in either an awake (n = 4) or anesthetized (n = 6) state in a custom-made holding tube.[63] For the anaesthetized scan, sedation was induced with 3% isoflurane in 3:7 O_2/air and maintained at 30 breaths per minute with 1 – 2% isoflurane. Body temperature was kept at 39ºC via a feedback-controlled warm waterbed (medres, Germany). For scanning during the awake state, subjects were head fixated in the holding tube. At the start of each scan, subjects received an intravenous (i.v.) injection of [^{18}F]FDG (~70 MBq in 500 μl) via a brachial vein catheter (Vasofix Safety G24) fixed with tape. Emission data were acquired for 60 min. Venous plasma glucose levels were measured after the scan with a handheld glucometer (On-Call GK Dual, ACON Laboratories Inc.), which we validated with a laboratory assay, see below. At the end of each scanning day, we performed a 10 min transmission scan using a[57] Co point source for attenuation correction. After scanning, pigeons were sacrificed and the heads were scanned for a structural MRI in a 7-T horizontal-bore small-animal scanner (Bruker BioSpec, 70/30 USR, Germany), with a single-loop 20 mm surface coil for signal detection and an 80 mm transmit quadrature birdcage resonator for radio-frequency transmission. To acquire MR data, Bruker ParaVision 5.1 software was used. T1-weighed anatomical images were acquired using multi-slice rapid acquisition (RARE) with the parameters: effective TE = 6.83 ms, TR = 100 ms, RARE factor = 2, number of average = 2, field of view = 21 x 28 x 31.5, slice thickness = 1 mm, spatial resolution = 0.07 x 0.07 x 0.07 mm, and dimensions = 400, 300, 450.

Validation of handheld glucometer

To validate the readings of the handheld glucometer used in this study, we took blood samples from the brachial vein of 8 pigeons (*Columba livia*). Samples were collected in ethylenediaminetetraacetic acid coated tubes and blood glucose levels were directly measured with the handheld device three times in each sample. Afterward, samples were centrifuged for 10 min at 1900 RCF at 4°C and plasma supernatant was stored at -80°C until further usage. Plasma glucose levels were acquired using the Glucose Colorimetric Assay Kit II (BioVision), strictly following the manual of the assay. Absorbance of the samples at 450 nm was measured with a Multiskan Fc photometer (Thermo Fisher Scientific). Based on the absorbance readings and a standard curve, plasma glucose concentrations were then calculated for each sample with the SkanIt software (Thermo Fisher Scientific).

Mean blood glucose concentrations measured with the handheld device were at 11.23 ± 0.82 mmol/L and glucose concentrations assessed with assay kit were at 12.58 ± 0.80 mmol/L. Both measured concentrations were within normoglycemic range for birds.[15] Statistical comparison (Wilcoxon signed-rank test, performed in SPSS Statistics, IBM) between the two measuring techniques revealed a significant difference ($z = -2.38$, $p = 0.017$), with slightly higher glucose values (12.56% on average) measured with the assay kit. This difference is still in the allowed variation range defined by the ISO norm 15197 for handheld glucometers used in humans.

Input function

The input function was established from plasma values.[12] Arterial blood was sampled from the brachial artery via a catheter (Vasofix Safety G24, B. Braun, Germany) fixed just before starting the scan. Blood was sampled continuously via the catheter elongated with a heparinised tube during the first 2 minutes and radioactivity was directly measured with a custom-made blood pump with an online detector set at a pulling rate of 1 ml/min.[62] The delay in measurement between the PET scanner and online blood detector was corrected for by dividing tube length by pulling velocity. The tube was then cut and after discarding 200 μl of catheter dead volume, discrete blood samples of 100 μl at 2, 5, 10, 20, 30, 45, and 60 min were taken. The manual blood samples were immediately put on ice. This reduces the inner blood transport of [^{18}F]FDG from plasma to red blood cells to negligible rates. Plasma was separated by centrifuging full blood for 12 min at 1500 *g* in a microcentrifuge (Centrifuge 5415 R, Eppendorf) and 40 μl plasma was used for analysis. Radioactivity was measured in both the full blood and plasma sample in a CompuGamma CS γ-counter (LKB/Wallac, Australia) and corrected for deadtime and radioactive decay. The plasma to full blood ratio of the radioactivity rates (counts/min) at each sampling time was calculated. The PET scanner, blood sampler and γ-counter were cross-calibrated.

Image processing

The emission scans were histogrammed into time frames (6 x 30, 3 x 60, 3 x 120 and 12 x 240 s) and fully 3D rebinned (span 3, ring difference 47) followed by OSEM3D/MAP reconstruction.[64] The resulting voxel size measured 0.38 x 0.38 x 0.80 mm. Next to the attenuation correction, scans were corrected for deadtime with a global estimate based on running deadtime average and radioactive decay. Images were analysed with the VINCI Software Tool.[65] The images were co-registered to a template structural MRI pigeon brain.

Please cite this article in press as: von Eugen et al., Avian neurons consume three times less glucose than mammalian neurons, Current Biology (2022), https://doi.org/10.1016/j.cub.2022.07.070

Kinetic modeling

The [^{18}F]FDG kinetics were determined with the two-tissue compartment model[11] (Figure 1B) that estimates four rate constants (K_1, transport from blood to brain; k_2, transport from the brain to blood; k_3, phosphorylation; k_4, dephosphorylation). Following Backes et al.,[12] parametric images of the rate constants were determined using a Powell algorithm for voxel-wise fitting of

$$C_T(t) = v_B C_B(t) + (1 - v_B)\left(A_- \int_0^t dt' C_P(t') e^{-r_-(t-t')} - A_+ \int_0^t dt' C_P(t') e^{-r_+(t-t')}\right) \quad \text{(Equation 1)}$$

with $C_T(t)$ representing tissue (in this case brain) radioactivity concentration, and

$$r_\pm = \frac{k_2 + k_3 + k_4}{2} \pm \frac{1}{2}\sqrt{(k_2 + k_3 + k_4)^2 - 4k_2k_4} \quad \text{(Equation 2)}$$

$$A_\pm = \frac{K_1}{r_- - r_+}(k_3 + k_4 - r_\pm) \quad \text{(Equation 3)}$$

where t is time in minutes after injection and v_B is the fractional blood volume in brain tissue. Since the exact blood volume for these pigeons was unknown, we ran the analysis with four different fractional blood volumes (3%, 4%, 5% and 6%) to investigate the effect of this variable on the final k-parameters and CMR_{glc}. We found that the different fractional blood volumes produced a negligible variation in the k-parameters and CMR_{glc}, see Table S1. The value of 5% is commonly used in rats and since the blood volume per unit brain weight was found to be the same in pigeon and rat,[66] it was also employed here for the main analysis. $C_B(t)$ expresses whole-blood radioactivity concentration, which was measured by continuous automatic sampling during the first two minutes after tracer injection, and manual sampling thereafter. The plasma radioactivity concentration C_P was directly measured in the manual samples and calculated for the period of continuous sampling as

$$C_P(t) = \frac{1}{a_v + (1 - a_v)(1 - e^{-kt})} C_B(t) \quad \text{(Equation 4)}$$

The parameters a_v and k were determined for each pigeon by fitting Eq. 4 to $C_B(t)$ and $C_P(t)$ measured in the manual samples. The net influx constant (K_i) for [^{18}F]FDG results from

$$K_i = \frac{K_1 \times k_3}{(k_2 + k_3)} \quad \text{(Equation 5)}$$

which translates into CMR_{glc} (μmol/100 g/min) via

$$CMR_{glc} = K_i \times \frac{1}{LC} \times C_{p,glc} \quad \text{(Equation 6)}$$

where $C_{P,glc}$ is the post-scan venous plasma glucose level and LC is the local lumped constant that describes the difference of glucose versus [^{18}F]FDG metabolism kinetics. Most commonly, a fixed value is taken for LC. It can be determined by model-independent and model-dependent methods and some variation is present in the mammalian literature.[16] This variation has been ascribed to methodological differences, or specificities of species or disease state.[17,18] Following Backes et al.,[12] here we employed a model-dependent method where the local LC is determined from the local kinetic rate constants of [^{18}F]FDG taking into account the different efficiencies in transport and phosphorylation of glucose and [^{18}F]FDG. It elaborates on the idea that disentangling the processes of transport and phosphorylation that are lumped together in the LC is more accurate. The difference between [^{18}F]FDG and glucose in transport and phosphorylation can be broken up into: $L_1 = K_{1,FDG}/K_{1,glc}$, $L_2 = k_{2,FDG}/k_{2,glc}$, and $L_3 = k_{3,FDG}/k_{3,glc}$. Based on Michaelis-Menten formalism, which describes enzyme kinetics, the ratio of difference between two substances that use the same system is a constant, because it describes ratios between constants.[18] This implies that there are fixed ratios of difference between glucose and [^{18}F]FDG in transport and phosphorylation, and including these in the model will allow for calculating region-dependent LCs for each individual pigeon.[18] The values for the separate ratios are: $L_1 = 1.48$, $L_2 = 1.48$ & $L_3 = 0.37$, and were found to be similar in both human and rat.[13,14] The local LC can then be calculated from the local kinetic rate constants of [^{18}F]FDG by:

$$LC = L_1\left(\frac{L_3}{L_2} + \left(1 - \frac{L_3}{L_2}\right)\frac{K_i}{K_1}\right) \quad \text{(Equation 7)}$$

QUANTIFICATION AND STATISTICAL ANALYSIS

Statistical analysis was executed with IBM Statistics SPSS 21 (IBM Corp, Released 2012, Armonk, NY). For all tests, a value was considered an outlier when it lay outside of the following range: 3rd or 1st quartile + or – 1.5 * interquartile range. Values are reported as mean ± standard deviation and results were significant if $p < 0.05$. Effect sizes were described with the partial eta squared (η^2). The injected [^{18}F]FDG dose and LC were compared between the awake and anaesthetized group with an independent t test. Both groups

Please cite this article in press as: von Eugen et al., Avian neurons consume three times less glucose than mammalian neurons, Current Biology (2022), https://doi.org/10.1016/j.cub.2022.07.070

met the assumption of normality and homogeneity of variance as tested with a Shapiro-Wilk and Levene's test, respectively, for both factors. For the LC values, one outlier was detected (case 645 of the i.v. anaesthetized group), which was excluded from further analysis of the LC. Differences in CMR_{glc} depending on brain region (forebrain, cerebellum or rest of brain) or group (i.v. awake/i.v. anesthetized) were assessed with a two-way mixed ANOVA. The within-subject variable was a repeated measure of ''Brain Region'', and the variable ''State'' was assessed as between-subject variables. The main effects were more closely analysed with a post hoc test with Bonferroni correction. All group values were normally distributed, as assessed with a Shapiro-Wilk test, and met the criterium of homogeneity of variance (Levene's test), and homogeneity of covariance matrices (Box's M test). The CMR_{glc} per neuron was calculated by dividing the average CMR_{glc}/mg of the awake state over neuron numbers/mg.[3] For this analysis we only used awake data since we are interested in the true neuronal energy budget without possible effects of anaesthesia.[8] The neuron numbers of the pigeon brain (n = 3) were retrieved from Olkowicz et al.[7] The neuronal energy budget of the pigeon was compared to mammalian data where both CMR_{glc} and neuron numbers were available.[3,9,37] Whole brain CMR_{glc} values in an awake state were available for mouse,[34] rat,[26–28] macaque,[35] baboon,[36] and human.[19,24,25]

Current Biology, Volume *32*

Supplemental Information

Avian neurons consume three times less glucose than mammalian neurons

Kaya von Eugen, Heike Endepols, Alexander Drzezga, Bernd Neumaier, Onur Güntürkün, Heiko Backes, and Felix Ströckens

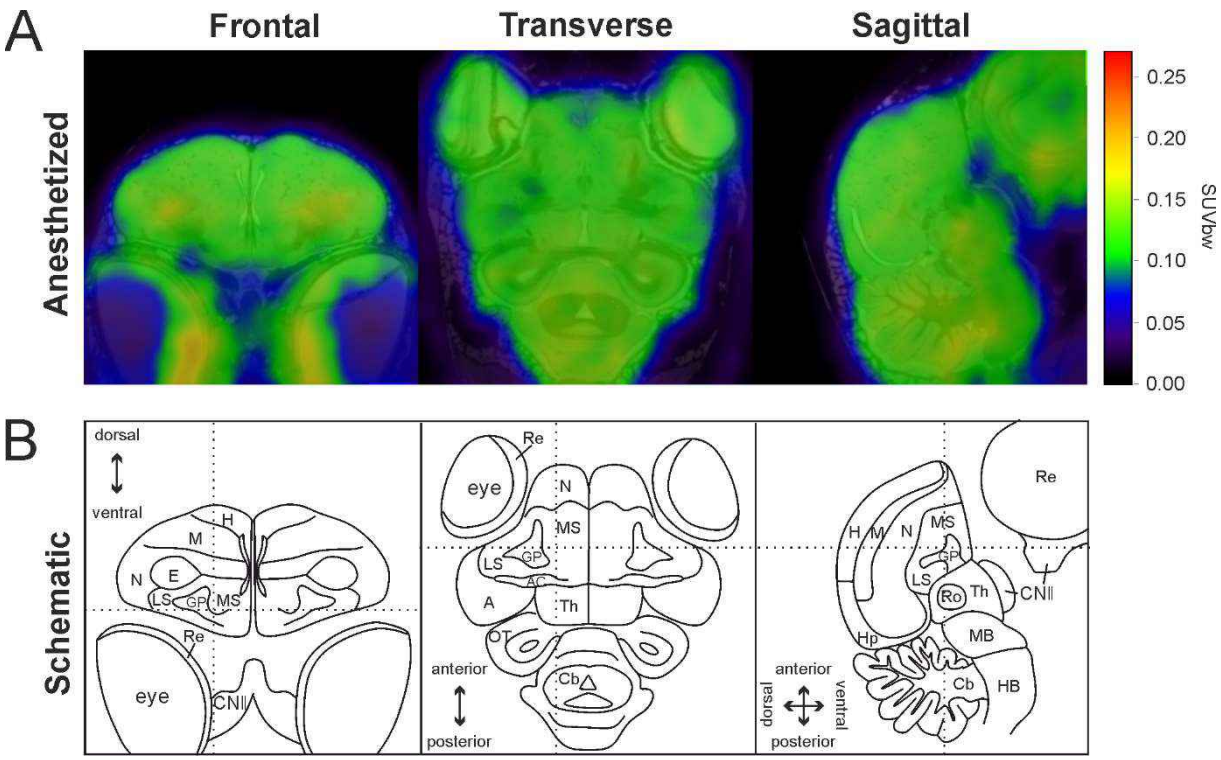

Figure S1. Example of ^{18}[F]FDG distribution in an anaesthetized state. Related to Figure 2A. (A) Cerebral [^{18}F]FDG activity in an anaesthetized state, see (B) for schematic overview of the brain. Dotted lines indicate the exact plane in frontal (left), transversal (middle), and sagittal (right) sections. The heat map represents standardized uptake value, corrected for body weight (SUVbw = image activity [Bq/ml] * bw [g] / injected dose [Bq]), with red indicating high and blue low levels of uptake. The distribution in the anaesthetized state is more diffuse compared to the awake state (compare Figure 2A). Most activity still resides in visual-related areas such as the retina and entopallium (one of the primary visual areas in the avian brain), although less prominent than in the awake state. In addition, we found relatively higher levels of activity in the brainstem and cerebellum. A = arcopallium, AC = anterior commissure, BS = brainstem, CNⅡ = second cranial nerve (optic nerve), Cb = cerebellum, E = entopallium, GP = globus pallidus, HB = hindbrain, LS = lateral striatum, M = mesopallium, MB = midbrain, N = nidopallium, OT = optic tectum, Re = retina, Ro = nucleus rotundus, RH = right hemisphere, Th = rest of thalamus.

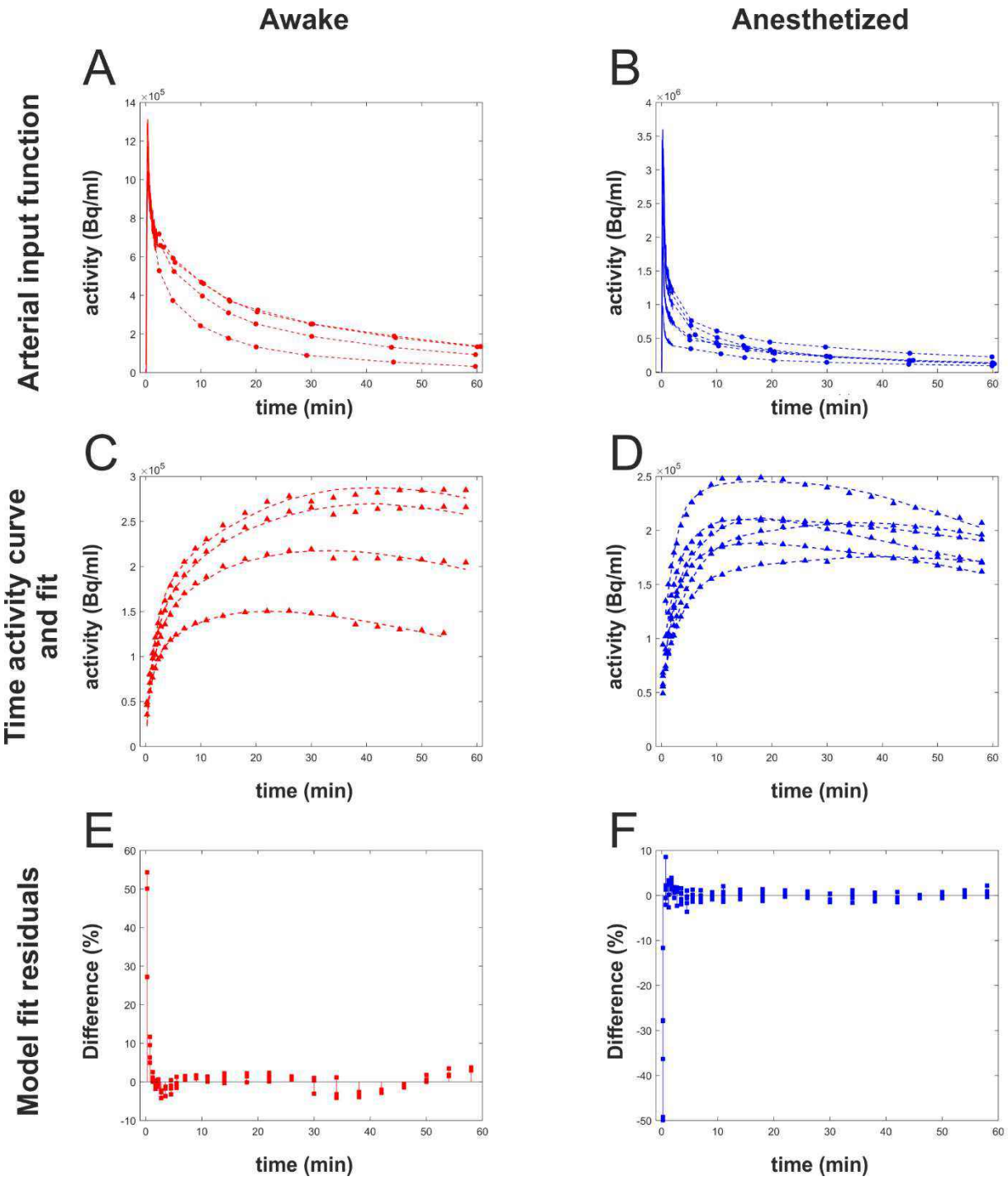

Figure S2. AIF, TAC, model fit and residuals for all pigeons. Related to Figure 2B-C. The AIF (A, B), TAC and model fit (C, D) and model fit residuals (E, F) for all pigeons in the awake (A, C, E) and anaesthetized (B, D, F) state. In both the awake and anaesthetized state the AIF is characterised by a sharp peak that slopes off within 1 minute and approaches a plateau. The peak in the anaesthetized state is higher compared to awake state. The TAC and model fit show a similar trajectory in both states, increasing sharply the first 10 – 20 minutes and sloping off to a plateau afterwards. The residuals show that the TAC and model fit have a high correspondence, differing by less than 5% at most time-points, except the first time-point where for all pigeons the percentage difference is higher.

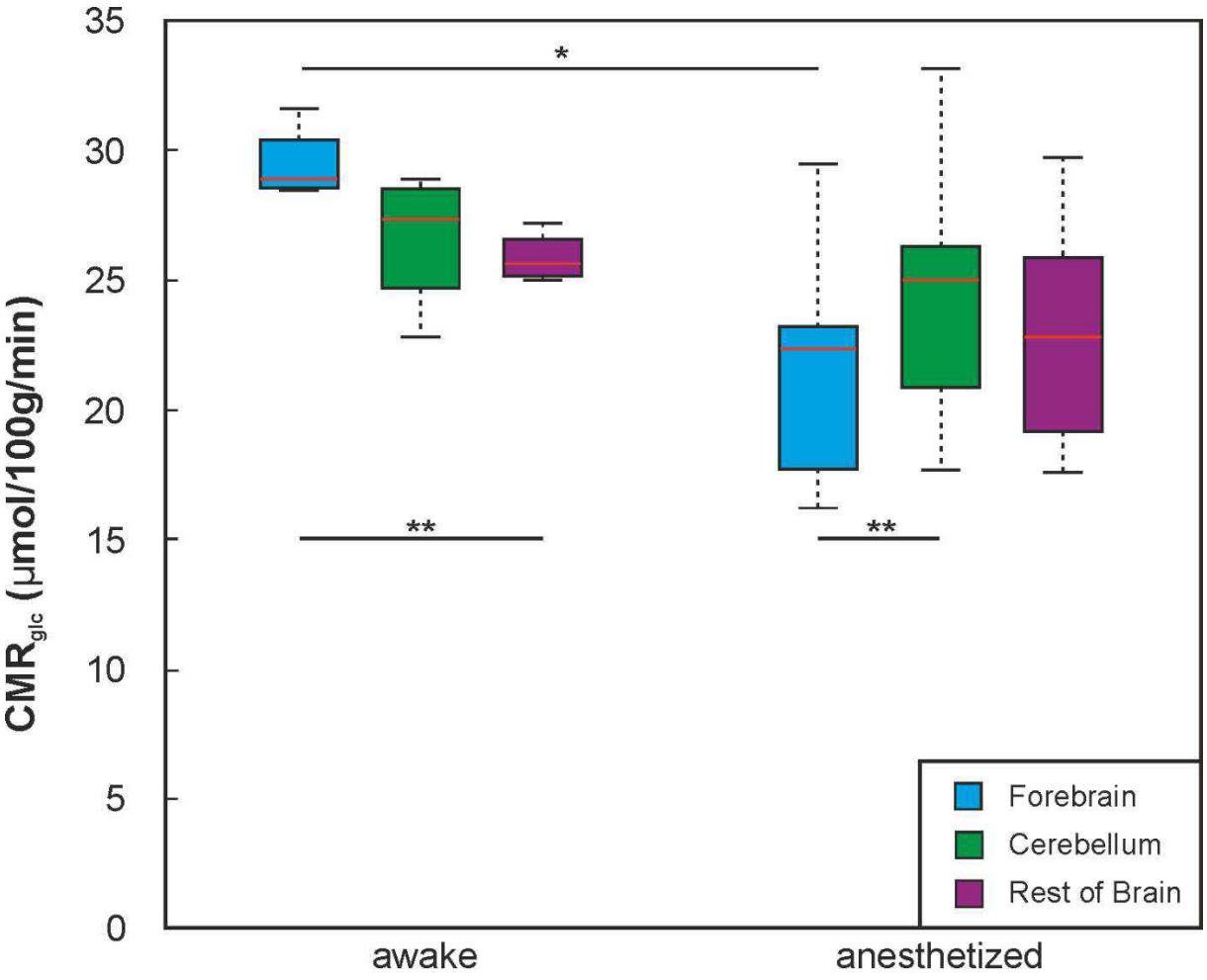

Figure S3. Boxplots of average CMR_{glc} of forebrain, cerebellum and the rest of brain per state. Related to Figure 2. CMR_{glc} differed between the states depending on the brain region ($F(2,16) = 24.95$, $p < 0.01$, $\eta^2 = 0.757$) with forebrain consuming more glucose in the awake state compared to anaesthetized state ($t(8) = 3.083$, $p = 0.015$). Moreover, brain regions differed in glucose consumption in both the awake ($F(2,6) = 9.872$, $p = 0.013$, $\eta^2 = 0.767$) and anaesthetized state ($F(2,10) = 22.513$, $p < 0.01$, $\eta^2 = 0.818$). Post hoc analysis with Bonferroni correction showed that in the awake state the forebrain consumed more glucose than the rest of brain ($p < 0.01$), and in the anaesthetized state the cerebellum used more glucose than the forebrain ($p < 0.01$). * = $p < 0.05$, ** = $p < 0.01$. CMR_{glc} = cerebral metabolic rate of glucose.

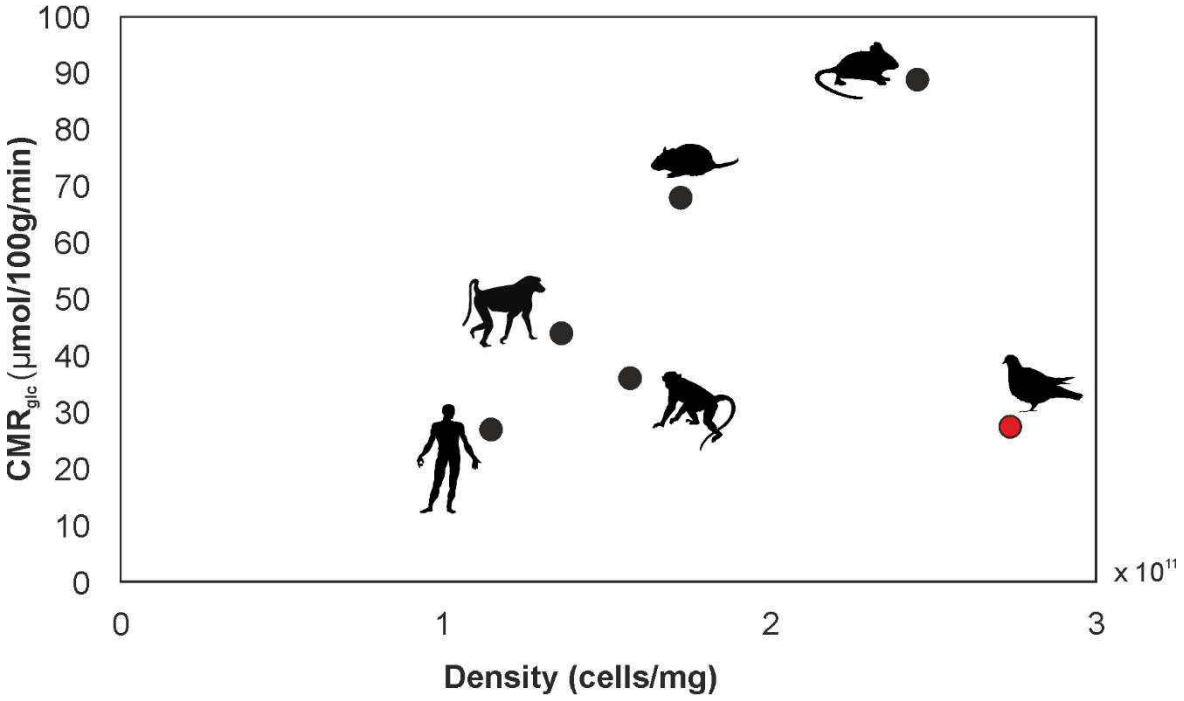

Figure S4. Scaling of mean specific CMR_{glc} and cell density in the whole-brain across species. Related to Figure 3. The graph depicts neuronal and glial cell densities per mg on the x-axis and µmol glucose consumption per 100 g per minute on the y-axis, representing CMR_{glc} per cell across different mammalian species and the pigeon. The pattern is highly similar to the CMR_{glc} per neuron (compare Figure 3). CMR_{glc} data were available for mouse [S1], rat [S2-S4], monkey [S5], baboon [S6] and human [S7-S9], and combined with estimated cell numbers [S10]. Cell numbers of the pigeon come from Olkowics et al. [S11]. Silhouettes were obtained from phylopic.org under public license.

State	Awake				Anaesthetized			
Blood volume	**3%**	**4%**	**5%**	**6%**	**3%**	**4%**	**5%**	**6%**
K1	0.061 ± 0.0034	0.060 ± 0.0035	0.059 ± 0.0036	0.058 ± 0.0037	0.046 ± 0.0084	0.045 ± 0.0083	0.044 ± 0.0083	0.043 ± 0.0083
k2	0.16 ± 0.0033	0.16 ± 0.0039	0.15 ± 0.0046	0.15 ± 0.0054	0.15 ± 0.018	0.15 ± 0.018	0.14 ± 0.019	0.14 ± 0.019
k3	0.063 ± 0.0052	0.064 ± 0.0051	0.064 ± 0.0046	0.065 ± 0.0048	0.058 ± 0.013	0.058 ± 0.013	0.059 ± 0.013	0.059 ± 0.013
k4	0.013 ± 0.00028	0.012 ± 0.00027	0.012 ± 0.00026	0.012 ± 0.00025	0.018 ± 000075	0.017 ± 0.0072	0.017 ± 0.0070	0.016 ± 0.0067
ki	0.017 ± 0.00078	0.017 ± 0.00078	0.017 ± 0.00078	0.018 ± 0.00078	0.012 ± 0.0017	0.012 ± 0.0027	0.012 ± 0.0017	0.012 ± 0.0017
LC	0.70 ± 0.023	0.70 ± 0024	0.71 ± 0.025	0.72 ± 0.026	0.66 ± 0.039	0.67 ± 0.038	0.68 ± 0.040	0.68 ± 0.042
CMRglc	27.48 ± 1.60	27.43 ± 1.66	28.29 ± 1.57	27.18 ± 1.56	23.64 ± 4.82	23.40 ± 0.048	23.15 ± 0.048	22.88 ± 0.048

Table S1. Overview of k-parameters and CMRglc. Related to Table 1. Since the exact brain blood volume percentage of pigeons is not known, four different whole blood volume percentages were modelled to investigate the effect of a varying blood volume percentage. We found that the whole blood volume has a negligible effect on the k-parameters and the final CMRglc in both the awake and anaesthetized state.

Species	Density (neurons / mg)	CMR_{glc} (µmol glucose/100 g/min)	Neuronal energy budget (CMR_{glc} / neuron)
Mouse	16×10^4	89	5.5×10^{-9}
Rat	10×10^4	68	6.5×10^{-9}
Monkey	7.3×10^4	36	4.9×10^{-9}
Baboon	7.4×10^4	44	6.0×10^{-9}
Human	5.7×10^4	26	4.6×10^{-9}
Pigeon	15×10^4	27	1.8×10^{-9}

Table S2. Neuronal densities, CMR_{glc}, and neuronal energy budget per species. Related to Figure 3. The graph in Figure 3 was generated from the neuronal density, CMR_{glc} and calculated neuronal energy budget for different mammalian species and the pigeon as estimated in this paper. CMR_{glc} data were available for mouse [S1], rat [S2-S4], monkey [S5], baboon [S6] and human [S7-S9], and combined with estimated neuron numbers [S10]. Neuron numbers of the pigeon come from Olkowics et al. [S11].

Supplemental references

S1. Bouilleret, V., Boyet, S., Marescaux, C., and Nehlig, A. (2000). Mapping of the progressive metabolic changes occurring during the development of hippocampal sclerosis in a model of mesial temporal lobe epilepsy. Brain Res. 852, 255–262.

S2. Nehlig, A., Preira de Vasconcelos, A., and Boyet, S. (1988). Quantitative autoradiographic measurement of local cerebral glucose utilization in freely moving rats during postnatal development. J. Neurosci. 8, 2321–2333.

S3. Waschke, K., Schrock, H., Albrecht, D.M., Van Ackern, K., and Kuschinsky, W. (1993). Local cerebral blood flow and glucose utilization after blood exchange with a hemoglobin-based O2carrier in conscious rats. Am. J. Physiol. - Hear. Circ. Physiol. 265.

S4. Levant, B., and Pazdernik, T.L. (2004). Differential effects of ibogaine on local cerebral glucose utilization in drug-naive and morphine-dependent rats. Brain Res. 1003, 159–167.

S5. Kennedy, C., Sakurada, O., Shinohara, M., Jehle, J., and Sokoloff, L. (1978). Local cerebral glucose utilization in the normal conscious macaque monkey. Ann. Neurol. 4, 293–301.

S6. Meguro, K., Blaizot, X., Kondoh, Y., Le Mestric, C., Baron, J.C., and Chavoix, C. (1999). Neocortical and hippocampal glucose hypometabolism following neurotoxic lesions of the entorhinal and perirhinal cortices in the non-human primate as shown by PET. Implications for Alzheimer's disease. Brain 122, 1519–1531.

S7. Sari, H., Erlandsson, K., Law, I., Larsson, H.B.W., Ourselin, S., Arridge, S., Atkinson, D., and Hutton, B.F. (2017). Estimation of an image derived input function with MR-defined carotid arteries in FDG-PET human studies using a novel partial volume correction method. J. Cereb. Blood Flow Metab. 37, 1398–1409.

S8. Sundar, L.K.S., Muzik, O., Rischka, L., Hahn, A., Rausch, I., Lanzenberger, R., Hienert, M., Klebermass, E.M., Füchsel, F.G., Hacker, M., et al. (2019). Towards quantitative [18F]FDG-PET/MRI of the brain: Automated MR-driven calculation of an image-derived input function for the non-invasive determination of cerebral glucose metabolic rates. J. Cereb. Blood Flow Metab. 39, 1516–1530.

S9. Huisman, M.C., van Golen, L.W., Hoetjes, N.J., Greuter, H.N., Schober, P., Ijzerman, R.G., Diamant, M., and Lammertsma, A.A. (2012). Cerebral blood flow and glucose metabolism in healthy volunteers measured using a high-resolution PET scanner. EJNMMI Res. 2, 1–9.

S10. Herculano-Houzel, S., Catania, K., Manger, P.R., and Kaas, J.H. (2015). Mammalian Brains Are Made of These: A Dataset of the Numbers and Densities of Neuronal and Nonneuronal Cells in the Brain of Glires, Primates, Scandentia, Eulipotyphlans, Afrotherians and Artiodactyls, and Their Relationship with Body Mass. Brain. Behav. Evol. 86, 145–163.

S11. Olkowicz, S., Kocourek, M., Luèan, R.K., Porteš, M., Fitch, W.T., Herculano-Houzel, S., Nemec, P., Lučan, R.K., Porteš, M., Fitch, W.T., et al. (2016). Birds have primate-like numbers of neurons in the forebrain. Proc. Natl. Acad. Sci. U. S. A. 113, 7255–7260.